ChemPhysChem

Chemistry Europe
European Chemical Societies Publishing

Accepted Article

Title: Insight into the Spin-Vibronic Problem of a Mixed Valence Magnetic Molecular Cell for Quantum Cellular Automata

Authors: Andrew Palii, Denis Korchagin, Sergey Aldoshin, J. M. Clemente-Juan, Shmuel Zilberg, and Boris Tsukerblat

To be cited as: *ChemPhysChem* 10.1002/cphc.202100312

Link to VoR: https://doi.org/10.1002/cphc.202100312

WILEY-VCH

Insight into the Spin-Vibronic Problem of a Mixed Valence Magnetic Molecular Cell for Quantum Cellular Automata

Andrew Palii,[*1] Denis Korchagin,[1] Sergey Aldoshin,[1] J. M. Clemente-Juan,[2] Shmuel Zilberg,[3] Boris Tsukerblat*[3,4]

[1]*Laboratory of Molecular Magnetic Nanomaterials, Institute of Problems of Chemical Physics of Russian Academy of Sciences, Chernogolovka, Moscow Region, 142432 Russia*

[2]*Instituto de Ciencia Molecular, Universidad de Valencia, 46980 Paterna, Spain*

[3]*University of Ariel, Materials Research Center*

[4]*Department of Chemistry, Ben-Gurion University of the Negev, 84105 Beer-Sheva, Israel*

* *Corresponding authors' e-mails*: andrew.palii@uv.es (A.P.); tsuker@bgu.ac.il (B.T.)

Abstract

The effects of the vibronic coupling in quantum cellular automata (QCA) based on the square planar mixed valence (MV) molecular cells comprising four paramagnetic centers (spin cores) and two excess mobile electrons are analyzed in the important particular case when the Coulomb energy gap between the ground antipodal diagonal-type two-electron configurations and the excited side-type configurations considerably exceeds both the one-electron transfer parameter (strong U – limit) and the vibronic stabilization energy. Under such conditions the developed model involves the second-order double exchange, the Heisenberg-Dirac-Van Vleck (HDVV) exchange and the vibronic coupling of the excess electrons with the molecular B_{1g} -vibration composed of four full-symmetric local vibrations. The latter interaction is shown to significant amplify the ability of the electric field produced by the driver-cell to polarize the excess electrons in the working cell, which can be termed "the effect of the vibronic enhancement of the cell-cell interaction". This effect leads to a redetermination of the conditions for switching between different spin-states, as well as to a significant change in the shapes of the cell-cell response functions. The obtained results demonstrate the importance of the vibronic coupling in all aspects (such as description of a free cell and cell-cell response) of the theory of molecular QCA based on MV clusters.

Keywords: quantum cellular automata; double exchange; mixed valence; vibronic coupling; intramolecular electron transfer ; exchange interaction; molecular magnetic clusters

Abbreviations:

QCA - Quantum Cellular Automata

DE-double exchange

HDVV exchange - Heisenberg-Dirac-Van Vleck exchange

MV- mixed valence

PKS model- Piepho, Krausz and Schatz model

JT - Jahn-Teller

1. Introduction

Quantum Cellular Automata (QCA) is presently a subject of the extensive studies at the borderline of chemistry, physics and material science. Interest to this topic is inspired by the prospects for the new kind of nanotechnology that is competitive to the traditional complementary metal–oxide–semiconductor (CMOS) technology for manufacturing of the logic elements for digital integrated circuits. As distinguished from CMOS elements, the QCA-based devices do not conduct electric current and so they can provide such important advantages as minimization of the heat release and the implementation of computations at very high switching rate. The pioneering concept underlying the filed [1-3] (reviewed in refs [4-6]) was based on the use of the cells composed of charged quantum dots to carry binary information as basic elements to design the logic gates [7-13].

These basic ideas were further developed through the proposal of using molecular cells instead of cells representing the arrays of quantum dots thus passing to the range of molecular electronics that would allow to utilize additional substantial advantages of QCA technology. Such advantages may include perspectives of controllable chemical engineering of molecular cells, possibility to reach extremely high density of the devices, which does not produce strong heat release and would operate at room temperature. The development of this field opened new horizons in the nanotechnological applications and computing with molecules.

Molecular systems suitable for playing role of cells in QCA devices should comprise two mobile electrons and admit the existence of two stable charge distributions that could carry binary information (**0** and **1**) and operate with this information when performing operations in the logic gates. Such properties are inherent in many compounds of mixed valence (MV) in which the role of the quantum dots is played by the redox sites linked by the bridging ligands mediating the electron tunneling. Driven by the development of the QCA area the targeted synthetic efforts during last years have led to the design of a number of organic and inorganic MV molecules for the purpose to get the systems suitable for the use as molecular cells for

QCA [14-29] (see also Ref. 30, 31] devoted to the quantum-chemical design of the cells). Two emphatic examples [32, 23] of molecular implementations of square-planar cells for QCA are shown in Fig. 1. These are the MV tetramers $[(cyclen)_4Ru^{II}_2Ru^{III}_2](pz)_4]^{10+}$ [32] and $[Fe^{II}_2Fe^{III}_2(L)_4]^{2+}$ [23] (cyclen = 1,4,7,10-tetraazacyclododecane, pz = pyrazine and H_2L = bis[phenyl(2-pyridyl)methanone]thiocarbohydrazone) which have been proposed as molecular cells that are able to encode binary information in the two diagonal charge configurations of the metal sites.

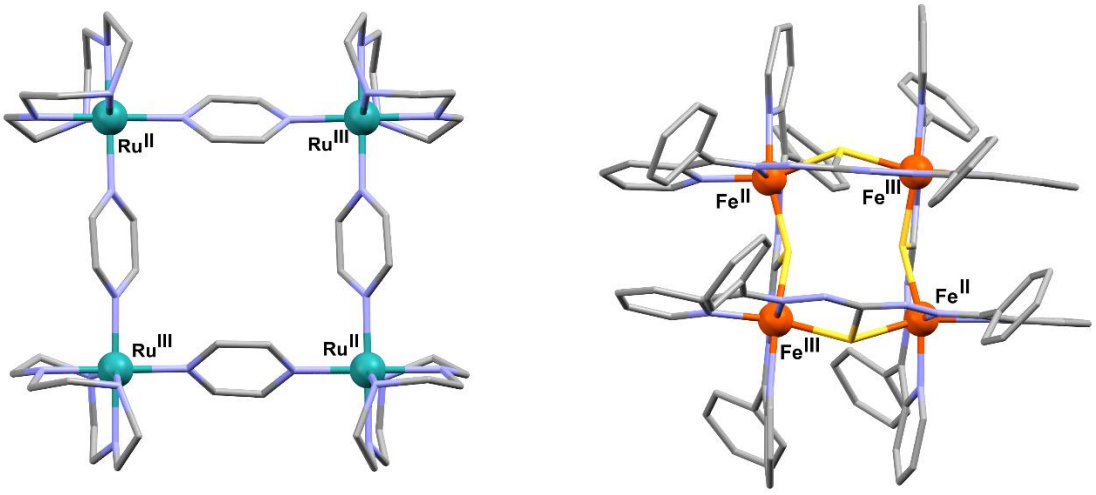

(a) (b)

Figure 1. Tetraruthenium $[Ru^{II}_2Ru^{III}_2]^{10+}$ [32] (a) and tetrairon $[Fe^{II}_2Fe^{III}_2]^{2+}$ [23] (b) MV squares which can serve for molecular expression of QCA. Coloring: gray, C; blue, N, yellow, S. Hydrogen atoms are omitted for clarity.

Along with the key requirement of bistability of the functioning (working) cell must be quickly switchable between the **0** and **1** configurations under the action of the so-called driver-cell, which means that the transitions between the two configurations cell should occur in a nonlinear abrupt manner. Actually, the molecular cell should have high polarizability in the electrostatic field induced by the driver cell.

The search and study of new MV systems satisfying these requirements remains a challenge today which have revived interest to the long-standing problem of intramolecular electron transfer that lies in the core of the concept of mixed valency and chemical transformations in general. The contemporary aspects of the theory of mixed valency have gained new influence associated with specific problems that have arisen in the field of molecular QCA.

Traditionally, the molecular cells based on MV clusters, as well as the cells composed of quantum dots, have the excess charges (electrons or holes) delocalized over the network of

diamagnetic sites. In particular, this is true for the two examples shown in Fig. 1. In our recent studies [33-35] we have proposed to substantially extend the class of cells by including MV systems in which the excess charges are delocalized over paramagnetic sites which, as applied to the MV clusters, are conventionally referred to as "spin cores". The presence of such spin cores along with the delocalized excess electrons is known to give rise to the double exchange (DE) that is sometimes also called "spin-dependent delocalization". In the short communication [33] the idea of using the MV dimers exhibiting DE as half-cells, which can be further combined to create bi-dimeric square cells for QCA and spin switchers has been proposed. As a further development of this idea we have recently considered a more complicated cell which represents square planar transition metal cluster of $d^2-d^2-d^1-d^1$-type comprising four spin cores (d^1- ions) and two excess electrons and exhibits combination of the DE and Heisenberg-Dirac-Van-Vleck (HDVV) exchange [34,35].

The model developed in articles [34,35] can be regarded as pure electronic one in the sense that only the electronic interactions are considered, namely, the DE, the HDVV exchange and the Coulomb interactions between the excess electrons, while the vibronic coupling has remained out of the scope of these studies. At the same time as it is well known from the theory of MV complexes the vibronic coupling can produce strong impact on the localization-delocalization phenomenon in MV systems and their properties [36-43]. Moreover, as has been demonstrated in a series of works [44-48] the vibronic coupling plays a decisive role in the adequate description of the functional properties of the cells. This shows that the development of the vibronic theory of MV square-planar cells comprising spin-cores represents a challenging problem.

In the present study we attempt to shed light on this issue through the detailed theoretical modelling of the isolated and interacting square planar-cells based on MV transition metal tetramer of the $d^2-d^2-d^1-d^1$ type. Along with the analysis of the functional characteristics of QCA based on multielectron cells, we thoroughly discuss the effects of the vibronic coupling and study a possibility of obtaining an additional spin switching function in the same device.

2. Summary of the results obtained in the framework of the electronic approach

The solution of the full vibronic problem involves two steps. At the first step, the electronic energy levels and the wave-functions of the cell are evaluated at fixed full symmetric nuclear configuration. This stage can be referred to as electronic problem. Then, at the second step one can evaluate the vibronic eigenvalues and eigenvectors by using the results obtained at the first

step. The electronic problem for the square planar cells comprising paramagnetic cores has been considered in details in Ref. [34]. Since the solution of the vibronic problem is substantially based on the solution of the electronic problem and in order to make the subsequent analysis of the vibronic effects self-consistent and more transparent, in this Section we give a brief description of some selected results (adapted to the aims of the present study and focused mainly on the visual concepts), which follow from the solution of the electronic problem.

The molecular cell under consideration is represented by a square planar tetranuclear MV cluster in which two excess electrons (or holes) are shared among four magnetic sites having spins s_0 ("spin cores"). For the sake of definiteness, we consider the cluster in which paramagnetic centers are represented by transition metal ions, and so the localized spins of the magnetic d^n and d^{n+1} ions in their Hund-type configurations are s_0 and $s_0 + 1/2$ correspondingly.

The solution of the electronic problem is relied on the simplified model that involves the following key interactions:

1) Coulomb repulsion between the two excess electrons that tends to remove the electrons from each other to the maximum distance allowed by the structure of the molecule, i. e. to put them in the vertices of the square lying on one or another its diagonal. As a result of this interaction the electronic levels prove to be discriminated into two Coulomb manifolds. The ground manifold arises from the two distant configurations (**1,3**) ≡ D_1 and (**2,4**) ≡ D_2 in which the electronic pair occupy the vertices of the square situated on its diagonals. The excited manifold comprises four neighboring charge dispositions (**1,2**), (**2,3**), (**3,4**), (**4,1**) in which the two excess electrons occupy vertices of the square situated on its sides (the adopted numeration of sites is indicated in Fig. 2). The antipodal configurations D_1 and D_2 form the low-lying group of levels, while the neighboring ones give rise to the excited levels with the energy U that is

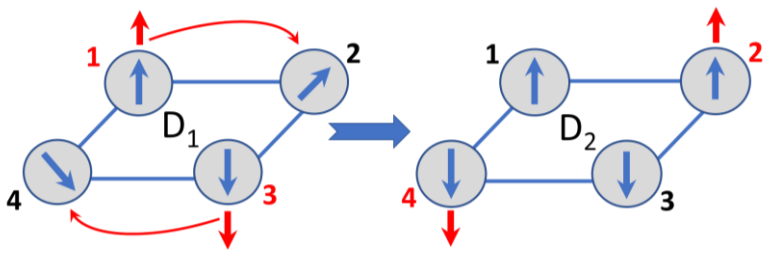

Figure 2. Scheme of the square-planar molecular cell comprising four spin cores and two excess electrons with indication of the two one-electron transfer processes giving

rise (in the sense of the second-order perturbation theory) to the two-step two-electron transfer occurring via excited Coulomb state and transforming the two antipodal diagonal-type configurations D_1 and D_2 into each other. Spins of the excess electrons are shown as red arrows, spin cores are dark blue arrows inside the sites shown by blue balls.

the parameter of the Coulomb repulsion between the two excess electrons;

2) the transfer of an excess electron from the occupied site d^{n+1} to its nearest neighboring spin core d^n (see Fig. 1 showing the transfer processes occurring along the sides, while the transfer pathways along the diagonals are forbidden), which leads to the kind of polarization of the spin-cores known as the double exchange [49-51];

3) Heisenberg-Dirac-Van-Vleck (HDVV) exchange interaction acting in different pairs of the magnetic ions (such as $d^n - d^n$, $d^n - d^{n+1}$ and $d^{n+1} - d^{n+1}$) which form the sides of the square (for exchange pathways we use the same assumption as for the electron transfer pathways, namely we assume that only the nearest neighboring ions can interact, while the diagonal-type exchange couplings are vanishing); 4) specifically, bearing in mind the QCA application of a MV bi-electronic unit as a building block for creating the logical gates, we include also in the model the interaction of a given cell ("working cell") with an external electrostatic field created by the polarized neighboring cell ("driver-cell"). Below we briefly discuss the named electronic interactions.

In the considered case of transition metal complexes, the Coulomb repulsion typically acts as a leading interaction playing a crucial role in the functionality of the QCA cell due to the fact that this interaction facilitates antipodal charge separations required to encode binary information. In this article we focus on this topical case (that is referred to as "strong U – limit"), when the Coulomb gap U considerably exceeds all other electronic interactions, partially in this case $U>>|t|$, where t is the parameter describing the one-electron transfer between the nearest neighboring sites. Consideration of this case allows us to apply the perturbation theory with Coulomb repulsion term acting as a zero order Hamiltonian while the electron transfer and the HDVV exchange terms playing the role of perturbation. Within this approximation one can deduce the effective Hamiltonian acting within the space of spin-states belonging to only two diagonal-type electronic distributions D_1 and D_2. Such truncated basis includes the following states:

$$\langle D_1 s_1^* s_3^* (S_{13}) s_2 s_4 (S_{24}) SM| \equiv \langle D_1 (S_{13}) (S_{24}) SM|, \quad (1)$$

$$\langle D_2 s_1 s_3 (S_{13}) s_2^* s_4^* (S_{24}) SM| \equiv \langle D_2 (S_{13}) (S_{24}) SM| \,. \quad (2)$$

The spin-functions are defined in the schemes of coupling of four site spins as defined in the notations in Eqs. (1) and (2) whose values are dictated by the electronic distribution. Here the "star" symbol indicates the presence of the excess electron on corresponding site, e. g. $s_1 = s_0$, $s_1^* = s_0 + 1/2$, etc. Each electronic state belonging to a definite distribution is specified by a pair of intermediate spins S_{13}, S_{34}, which are coupled to give a total spin S.

Each one-electron transfer process (caused by the one-electron interactions, mainly, by the kinetic energy of the excess electron) changes the distribution of the excess electrons and also gives rise to the change of the Coulomb energy of the cell by the amount of U. In order to transform the ground Coulomb configurations D_1 and D_2 into each other one needs two one-electron jumps $(\mathbf{1},\mathbf{3}) \rightarrow (\mathbf{2},\mathbf{3}) \rightarrow (\mathbf{2},\mathbf{4})$, i. e. the transition from D_1 to D_2 occurs via the excited charge configuration $(\mathbf{2},\mathbf{3})$ as shown in Fig. 1. In the considered case of $U>>|t|$ such transition can be regarded as a result of the effective two-electron transfer (Fig. 1) described by the effective transfer (or DE) parameter $\tau = t^2/U$ provided that the application of the second-order perturbation theory is justified. The effective DE Hamiltonian acts within the truncated spin basis defined by Eqs. (1) and (2) giving rise to the off-diagonal (resonance) matrix elements of the Hamiltonian matrix, which are proportional to τ and connect the spin-states belonging to D_1 and D_2.

As distinguished from the systems with localized spins, a feature of MV compounds is that the network of the HDVV exchange interaction is not solely determined by the mutual disposition of the interacting spins but also depends on the distribution of the excess electrons within which such interaction is considered because such distribution defines the positions of the d^n and d^{n+1} ions. As distinguished from the DE that mixes different electronic distributions, the HDVV exchange acts within each such distribution for which it can be written as:

$$\widehat{H}_{ex}(D_i) = \sum_{\langle k,l \rangle} J_{kl}(D_i)\, \hat{\boldsymbol{s}}_k \hat{\boldsymbol{s}}_l, \quad (3)$$

where the exchange parameters J_{kl} and the spins s_i of the sites depend on D_i, summation $\langle k,l \rangle$ runs over all pairs of nearest neighboring spins. Therefore $\widehat{H}_{ex}(D_i)$ can be thought as i^{th} diagonal (defined in the spin basis D_i) block of the full matrix of the HDVV exchange. In the initial exchange Hamiltonian defined in the full space comprising both ground and excited Coulomb configurations the HDVV exchange is described by three different exchange parameters: $J(d^n - d^n)$, $J(d^n - d^{n+1})$ and $J(d^{n+1} - d^{n+1})$. However, when the strong U-

limit occurs, the effective perturbational Hamiltonian acts in the restricted space of only two diagonal-type configurations D_1 and D_2 in which the d^{n+1} and d^n ions alternate and so in this limit and under adopted assumption that only nearest neighboring spins interact, the exchange coupling is described by the only exchange parameter $J(d^n - d^{n+1}) \equiv J$. Here, as in paper [34], this parameter is considered to be negative (antiferromagnetic HDVV exchange), that seems to be the most typical case in transition metal clusters.

Finally, the action of the polarized driver-cell on the working cell can be described by the parameter uP_{dc}, where u is the characteristic intracell Coulomb energy [45], which depends on the intra- and intercell distances and on the relative permittivity of intercell media, while P_{dc} is the polarization of the driver-cell (explicit expressions are given in Ref. [45]). Both polarization P_{dc} of the driver-cell that is assumed to be tunable in a controllable way, and polarization P_{wc} of the working cell that is induced due to its interaction with the electrostatic field created by the polarized driver-cell can be defined as a scalar quantity P [1, 2] showing to which extent the excessive charges are located in antipodal diagonal positions (**1,3)** or (**2,4**), namely:

$$P = \frac{(\rho_1+\rho_3)-(\rho_2+\rho_4)}{\rho_1+\rho_3+\rho_2+\rho_4}, \quad (4)$$

where ρ_i is the i^{th} site occupation probability. For example, when the sites **2** and **4** are empty and each of positions **1** and **3** each contains excess electron ($\rho_2 = \rho_4 = 0,\ \rho_1 = \rho_3 = 1$) the cell is fully polarized in the position (**1, 3)** and consequently $P = +1$, etc.

The energies of tetrameric MV molecular square cell of the $d^2 - d^2 - d^1 - d^1$-type evaluated in the strong U - limit are listed in Table 1. Due to the fact that the second-order DE mixes the spin states pertaining to different diagonal-type distributions, the spin eigen-functions are in general superpositions of such states, although in some cases due to high symmetry of the system the states with a certain D_i prove to be the exact eigen-functions as can be seen from Table 1.

Table 1. Energies of and spin-states (spin projection quantum number M is omitted) of the tetrameric MV molecular square cell of the $d^2 - d^2 - d^1 - d^1$-type evaluated in the strong U - limit (configurations D_1 and D_2) as functions of J, τ, u and P_2. Notation $D_1(1)(1)2$, $D_2(1)(1)2$, *etc.* means that the spin-functions are the superpositions of the spin states with localizations D_1 and D_2, the corresponding coefficients are not given for the sake of brevity.

$D_i(S_{13})(S_{24})$S	Energies
$D_1(2)(1)3$	$-4J-4\tau-uP_{dc}$
$D_2(1)(2)3$	$-4J-4\tau+uP_{dc}$
$D_1(2)(1)2$	$(4J-5\tau-2uP_{dc})/2$
$D_2(1)(2)2$	$(4J-5\tau+2uP_{dc})/2$
$D_1(2)(0)2$	$-3\tau-uP_{dc}$
$D_2(0)(2)2$	$-3\tau+uP_{dc}$
$D_1(1)(1)2,\ D_2(1)(1)2$	$\left(-4J-7\tau\pm2\sqrt{4\tau^2+u^2P_{dc}^2}\right)/2$
$D_1(2)(1)1$	$(12J-3\tau-2uP_{dc})/2$
$D_2(1)(2)1$	$(12J-3\tau+2uP_{dc})/2$
$D_1(1)(1)1,\ D_2(1)(1)1$	$\left(4J-5\tau\pm2\sqrt{4\tau^2+u^2P_{dc}^2}\right)/2$
$D_1(1)(0)1,\ D_2(1)(0)1$	$-3\tau\pm\sqrt{6\tau^2+u^2P_{dc}^2}$
$D_1(0)(1)1,\ D_2\ (0)(1)1$	$-3\tau\pm\sqrt{6\tau^2+u^2P_{dc}^2}$
$D_1(1)(1)0,\ D_2\ (1)(1)0$	$4J-2\tau\pm\sqrt{4\tau^2+u^2P_{dc}^2}$
$D_1(0)(0)0,\ D_2(0)(0)0$	$-3\tau\pm\sqrt{9\tau^2+u^2P_{dc}^2}$

By setting $P_{dc}=0$ in the expressions in Table 1 one obtains the eigenvalues for the free cell, which are shown in Fig. 3 in the form of electronic correlation diagram. It follows from the diagram that depending on the relative strength of the effective second order DE and the antiferromagnetic HDVV exchange the free cell can possess three different ground spin-states. Thus, at relatively strong DE the ground state is an orbital singlet with $S_{13}=S_{34}=0$, S=0 that is the linear combination of the states belonging to D_1 and D_2 configurations. This state is labeled as 1 in Fig. 3 and its energy is given in the last line of Table 1. For moderate $|J|/\tau$ values the ground state is an orbital singlet with $S_{13}=S_{34}=1$, S=0 that is also the linear combination of the D_1 and D_2- confugurations states (state 2 in Fig. 3 and penultimate line of Table 1). Finally at relatively weak double exchange the ground state is that with S =1. This state is an orbital doublet having the components $D_1(2)(1)1$ and $D_2(1)(2)1$.

The remarkable feature of this energy pattern is that the effect of the DE itself is antiferromagnetic (the ground state at relatively strong double exchange is the spin singlet). This contradicts with the well-known effect of the DE in the MV dimers in which the DE always tends to produce ferromagnetic spin alignment [49-51]. The unusual antiferromagnetic effect of the DE in the square planar tetramers with two excess electrons has been explained by the fact that the two excess electrons always keep their spins antiparallel in

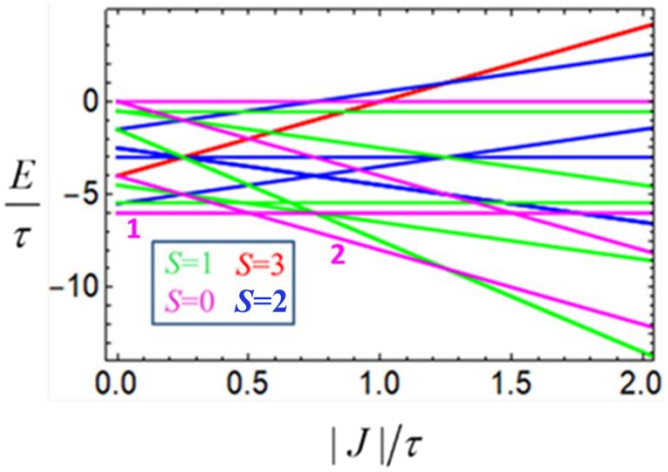

Figure 3. Electronic correlation diagram of energy levels of free square-planar tetrameric $d^2 - d^2 - d^1 - d^1$-type cell calculated for the limiting case of strong intra-cell Coulomb repulsion. The S=0 - states with $S_{13} = S_{34} = 0$ and $S_{13} = S_{34} = 1$ are labelled as 1 and 2 respectively.

course of delocalization and hence they produce mutually compensated impacts on the overall polarization of the four spin cores [35].

When the working the cell is exposed to a quadrupole electrostatic field produced by the polarized driver-cell such field produces drastically different effects on the orbital doublets (localized states) and the orbital singlets (delocalized states) as can be seen by inspecting the expressions in Table 1. Indeed, it produces strong linear Stark splitting of the orbital doublets, while the effect that field produces on the orbital singlets proves to be much weaker and consists in the mixing of the orbital singlets having opposite parities (the states in Table 1 whose expressions for energies contain the square root).

As distinguished from the orbital doublets describing fully localized electronic pair, the orbital singlets correspond to the delocalization of such pair over two diagonal positions. As a result, the orbitally nondegenerate states should exhibit significantly lower sensitivity to the quadrupole field created by polarized driver-cell. This means that if, for example, at zero field (i.e., at $P_{dc} = 0$) one of the orbital singlets with S = 0 (state 1 or 2 according to the notation

adopted in Fig. 3) is the ground state, at $P_{dc} \neq 0$ spin switching may occur. As a result, the ground state can become a state with S = 1, which is an orbital doublet with components $D_1(2)(1)1$ and $D_2(1)(2)1$, which should exhibit linear Stark splitting, leading to a strong stabilization of one of these (depending on the sign of P_{dc}) component.

It should be also noted that the orbital and spin singlets 1 and 2 undergo different stabilizations in the applied quadrupole field. Indeed, as one can see from the expressions listed in Table 1, at $P_{dc} = 0$ the two orbital singlets with $S_{13} = S_{34} = 0$, $S = 0$ are stronger separated from each other (by the energy gap 6τ) than the orbital singlets with $S_{13} = S_{34} = 0$, $S = 1$ (gap 4τ) and so the state 2 undergoes stronger stabilization in the field than the state 1 because of stronger Stark mixing of the two states having opposite parities. This means that if initially (at $P_{dc} = 0$) the ground state of the cell is the state 1 it can switch to the ground state 2 at some critical field. Note that the latter switching is not accompanied by the change of *S* because states 1 and 2 both are spin-singlets.

Finally, in the case of relatively strong double exchange, when $|J|/\tau$ is negligibly small, we have predicted the field induced spin-switching from the state with *S*=0 (state 1) to the state with *S*=3. The ability of the cell to be switched to the state with *S*=3 which cannot appear to be the ground state of the free cell in the framework of electronic approach is explained by the fact that at $P_{dc} = 0$ the state with *S*=3 represents the orbital doublet with components $D_1(2)(1)3$ and $D_2(1)(2)3$ which undergoes strong linear Stark splitting and at strong DE (left part of correlation diagram in Fig. 3) this state proves to be separated from the ground state 1 by lesser gap than the state 2.

3. Vibronic coupling in a tetrameric cell

In order to reveal the main consequences of the vibronic coupling we will use the conventional and simplest Piepho-Krauzs-Schatz (PKS) vibronic model repeatedly described in literature [38-43]. This model makes it possible to simplify and visualize the examination of molecular MV cell and at the same time to focus this examination just on those aspects which seem to be of crucial importance for the proper description of the functional properties of the QCA cells.

The basic assumption of the PKS model is that a MV molecular system can be conventionally subdivided into fragments accommodating mobile charge (redox sites) connected through the charge transfer processes and exhibiting well localized independent vibrations encompassing the region of the sites. Typically, it is assumed that the excess

electrons are effectively coupled to the fully symmetric (so-called "breathing") local modes whose explicit forms are determined by the nature of the system and the definition of the redox site in a complex structure. In the considered transition metal complexes, the redox sites are formed by the metal ions, which are assumed not to participate in the vibrations, and their nearest ligand environments, whose vibrations (at fixed positions of metal ions) just play role of the breathing modes. The breathing vibrations are assumed to have unique bare frequency ω that is assumed to be independent of the number of the site and its occupation by the excess electron (i. e. the value of ω is the same for d^n and d^{n+1} sites).

As a next step one can pass from the full-symmetric local modes described by the vibrational coordinates q_1, q_2, q_3 and q_4 to the symmetry adapted molecular vibrations which are classified accordingly to the irreducible representation of the $\mathbf{D}_{4h}$ point group and span irreducible representations A_{1g}, E_u and B_{1g}. Figure 4 shows the images of these symmetry adapted vibrations. The fully symmetric molecular vibration with the coordinate $q_{A_{1g}}$ represents

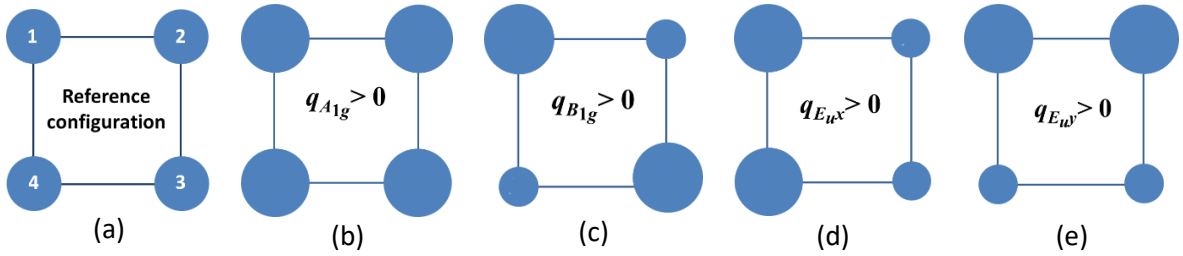

Figure 4. Pictorial representation of the symmetry adapted vibrational coordinates of the square-planar unit in the PKS model, all $q_\alpha > 0$: reference configuration (a); full-symmetric vibration A_{1g} (b); B_{1g}-vibration (c); the two components of E_u vibrations (d) and (e) . The balls mimic the surroundings (first coordination spheres) of the redox sites: large and small balls symbolize expanded and compressed surrounding correspondingly, medium balls-reference configuration.

equal expansion or contraction of the coordination environments of the four redox centers, the coordinate $q_{B_{1g}}$ describes the out-of-phase even-type vibration consisting in the expansion of the two coordination spheres belonging to one diagonal accompanied by the contraction of the spheres lying on another diagonal of the cell, finally, the coordinates $q_{E_u x}$ and $q_{E_u y}$ describe odd-type out-of-phase E_u - vibrations in course of which the coordination spheres belonging to one side of the square cell are expanded while the spheres belonging to opposite side are contracted. As we will see later on the explicit forms of these active vibrations are interrelated with the specific electron transfer processes in molecular cell.

It is intuitive (and can be rigorously proven) that only the B_{1g} − type vibration with the coordinate

$$q_{B_{1g}} \equiv q = \frac{1}{2}(q_1 + q_3 - q_2 - q_4) \ . \quad (5)$$

is relevant to the considered strong *U*-limit, while all other vibrations should be ruled out. Indeed, just this vibration involves the sites at the vertices of the square disposed on its diagonals (Fig. 4) and so only this vibration is interrelated with the charge conversion between the two antipodal configurations D_1 and D_2, while the vibrations of E_u -type involve the pairs of sites situated on the sides of the square and so they act only within the excited side-type configurations. This is illustrated in Fig. 5a from which one can see that the sites 1 and 3 initially (in D_1 configuration) occupied by the excess electrons and thus expanded because of negatively charged ligand surroundings of the metal ions, undergoes compression upon $D_1 \rightarrow D_2$ -transformation, and vice versa, the initially compressed sites 2 and 4 are getting

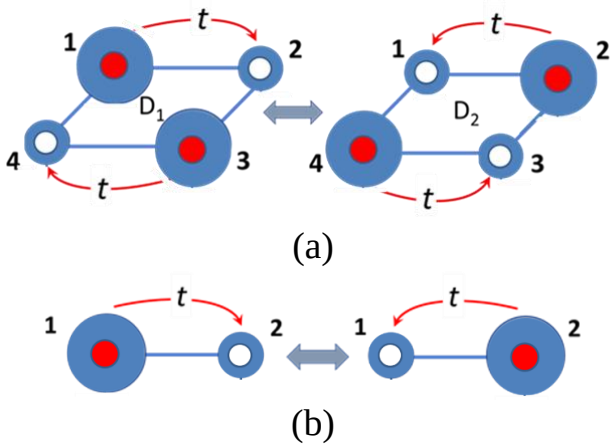

Figure 5. Illustration of interrelation between the out-of-phase B_{1g} −type PKS vibration and the effective two-electron second-order transfer in a square-planar MV tetramer comprising two excess electrons (a) and between the odd out-of-phase vibration and the one-electron transfer in a MV dimer (b). White balls - spin cores, red balls – metal ions comprising excess electrons, blue balls - ligand environments of the metal ions.

expanded (at least in ionic model) since they contain excess electrons in the D_2 configuration.

Note that the B_{1g} −type PKS vibration in a square-planar tetramer with two excess electrons plays the same physical role as the odd-type out-of-phase PKS vibration with the coordinate

$$q_- = (q_1 - q_2)/\sqrt{2} \quad (6)$$

in a MV dimer. The latter vibration that has been widely discussed in the literature [40] is directly interrelated with one-electron transfer in a MV dimer (Fig. 5b). The analogy of the roles of these two kinds of vibrations becomes clear from comparison of Figs. 5a and 5b.

Being localized on the site i the excess electron interacts with the local vibration q_i and such vibronic coupling results in the change of the site energy by the amount of υq_i, where υ is the vibronic coupling parameter. As far as the PKS model deals with only local breathing modes or symmetry adapted molecular vibrations composed of these local modes, Eq. (5), the vibronic coupling operator proves to be diagonal with respect to the quantum numbers of electronic distributions. Moreover, since the vibronic coupling is spin-independent it is diagonal with respect to all sets of intermediate and full spin quantum numbers. One can prove that in the considered case of strong *U*-limit this gives the following expression for the matrix elements of the vibronic coupling operator $\hat{V}$:

$$\left\langle D_i\ (S_{13})(S_{24})S\ M\middle|\hat{V}\middle|D_i\ (S'_{13})(S'_{24})S'M'\right\rangle \qquad (7)$$

$$= \pm\upsilon\ q\ \delta(S_{13},S'_{13})\ \delta(S_{24},S'_{24})\delta(S,S')\delta(M,M'),\qquad i=1,2,$$

where the signs "+" and "− "are related to the configurations D_1 and D_2 respectively, and $\delta(S,S')$, etc. are the Kronecker δ-symbols.

It follows from Eq. (7) that in the considered case of one-mode vibronic problem arising for the states belonging to the ground Coulomb manifold of the cell, the vibrationally-dependent part of the Hamiltonian can be obtained as follows:

$$\hat{H}_{vib} = \frac{\hbar\omega}{2}\left(q^2 - \frac{\partial^2}{\partial q^2}\right)\begin{pmatrix}1 & 0\\ 0 & 1\end{pmatrix} + \upsilon\begin{pmatrix}q & 0\\ 0 & -q\end{pmatrix} \equiv \hat{H}_0 + \hat{V}. \qquad (8)$$

where the term $\hat{H}_0$ is the Hamiltonian of the free harmonic B_{1g}-vibration with the frequency ω that includes operators of elastic (first term) and kinetic (second term) energies. The Hamiltonian, Eq. (8) is defined in the matrix form as a basis set the wave-functions $\langle D_i\ (S_{13})(S_{24})SM|\ (i=1,2)$. More exactly, Eq. (8) provides the 2×2-block of the full matrix that corresponds to a definite spin state and is restricted to the two antipodal configurations D_1 and D_2.

As we could see the vibrational space of the tetrameric cell involves three active non-symmetric vibrations B_{1g} and E_u. An important clarification needs to be made concerning the applicability of the one-mode Hamiltonian, Eq. (8), acting within the restricted space of the ground Coulomb manifold (configurations D_1 and D_2) that deals with the one mode B_{1g}. It is

to be underlined that such Hamiltonian is valid only provided that the energies corresponding configurations D_1 and D_2 are well separated from the excited ones. This means that the vibronic coupling is weak as compared with the intracell Coulomb interaction. Combining this requirement with the definition of the strong U - limit, one can say that the present vibronic approach is valid if the inequalities $\upsilon^2/(2\hbar\omega), |t| \ll U$ are fulfilled, when $\upsilon^2/(2\hbar\omega)$ is the vibronic stabilization energy (see Section 4).

It is worth noting that in a general case when the above inequalities are violated, the vibronic problem proves to be much more complex in the sense that in addition to the interaction of the access electrons with the B_{1g} - type PKS vibration one also has to consider the interaction of these electrons with the two odd E_u -type PKS modes [47]. This gives rise to the three-mode vibronic problem, which requires not only to enlarge the electronic space including along with the diagonal-type electronic configurations (ground Coulomb manifold) also the side-type configurations (excited Coulomb manifold), but also much larger vibrational space composed of the wave-functions of three-dimensional harmonic oscillator. This general case of arbitrary relationship between the key parameters of the cell is out of the scope of this paper and will be considered elsewhere.

4. Semiclassical analysis of the vibronic effects in the magnetic QCA cell

To solve the vibronic problem, one should add to the vibronic part of the Hamiltonian the matrices of the electronic interactions defined within the same basis. For the considered case of $d^2 - d^2 - d^1 - d^1$-type system these matrices have been deduced in Ref. [34], and their eigenstates are just those presented in Table 1. At the first stage we will treat the vibronic problem within the semiclassical adiabatic approximation that in some cases (described in Ref. [48] in detail) suffers from imprecision but in general provides reliable and visual results.

To evaluate the adiabatic potentials as functions of the coordinate q one has to neglect the vibrational kinetic energy term in the vibrationally-dependent Hamiltonian, Eq. (8). Since in the present case of one-mode vibronic problem for each spin-state we are dealing with the 2×2 matrix the expressions for the adiabatic potentials can be found analytically. Depending on the specific of the given spin-state we will use two kings of labelling for the pairs the adiabatic potential curves (or, in other words, for two branches of the adiabatic potential), namely they will be specified either by the symbol of electronic distribution (D_1 or D_2) and the set of spin quantum numbers $S_{13}, S_{24}S$ like $U_{D_i}((S_{13}, S_{24})S, P_2|q)$ in the case of localized orbital doublets, or by the signs $\pm$ such as, for example $U_{\pm}((S_{13}, S_{24})S, P_2|q)$ provided that the D_i – states are mixed (delocalized orbital singlets).

For the actual four spin-states with *S*=3, *S*=1 and *S*=0 (states 1 and 2), which under some conditions described in Section 2 can be the ground states of the tetramer, one obtains the following expressions for the adiabatic potentials of the working cell of $d^2 - d^2 - d^1 - d^1$-type subjected to the field of polarized driver-cell:

$$U_{D_1}((2,1)3, P_2|q) = \frac{\hbar\omega}{2}q^2 - 4J - 4\tau + (\upsilon q - uP_2), \quad (9)$$

$$U_{D_2}((1,2)3, P_2|q) = \frac{\hbar\omega}{2}q^2 - 4J - 4\tau - (\upsilon q - uP_2), \quad (10)$$

$$U_{D_1}((2,1)1, P_2|q) = \frac{\hbar\omega}{2}q^2 + 6J - \frac{3\tau}{2} + (\upsilon q - uP_2), \quad (11)$$

$$U_{D_2}((1,2)1, P_2|q) = \frac{\hbar\omega}{2}q^2 + 6J - \frac{3\tau}{2} - (\upsilon q - uP_2), \quad (12)$$

$$U_{\pm}((1,1)0, P_2|q) = \frac{\hbar\omega}{2}q^2 + 4J - 2\tau \pm \sqrt{4\tau^2 + (\upsilon q - uP_2)^2}, \quad (13)$$

$$U_{\pm}((0,0)0, P_2|q) = \frac{\hbar\omega}{2}q^2 - 3\tau \pm \sqrt{9\tau^2 + (\upsilon q - uP_2)^2}. \quad (14)$$

Let us first discuss the adiabatic potentials of a free cell, for which purpose one should set $P_{dc} = 0$ in in Eqs. (9)-(14). Inspecting the shapes of the adiabatic potentials of a free cell one can see that it is necessary to distinguish two physically different situations which appear depending on the specific of the electronic state, namely, the case of the static Jahn-Teller (JT) effect occurring for localized orbital doublets and the case of pseudo-JT effect arising when the two orbital singlets are mixed by the vibronic coupling operator giving rise to the dynamic vibronic problem. From the point of view of the QCA functionality these two cases correspond to different abilities of the working cell to be polarized by the electrostatic field of the driver-cell.

The case of static JT effect is represented by the orbital doublets with *S*=3 and S=1. Considering for example the adiabatic potentials for *S*=3 obtained by substituting $P_{dc} = 0$ into Eqs. (9) and (10) one can present them as follows:

$$U_{D_1}\big((2,1), 3|q\big) = -4J - 4\tau + \frac{\hbar\omega}{2}(q + q_0)^2 - \Delta E, \quad (15)$$

$$U_{D_2}((1,2)3|q) = -4J - 4\tau + \frac{\hbar\omega}{2}(q - q_0)^2 - \Delta E. \quad (16)$$

It is seen that the adiabatic potentials in this case are represented by the two intersecting parabolas whose minima are located at $q = \pm q_0$ with $q_0 = \upsilon/\hbar\omega$, while $\Delta E = \upsilon^2/2\hbar\omega$ represents the vibronic stabilization energy defined as a difference between the adiabatic potential value in the point of intersection of the two curves and its value in the minima. Such

form of the adiabatic potential is an evidence of the static JT effect in the orbital doublet with *S*= 3, which has electronic energy $-4J-4\tau$. In this case the electronic pair is fully localized in each minimum leading to the formation of one of the two stable antipodal (diagonal-type) charge configurations. The same conclusion is valid for the two states with *S*=1 having electronic energy $6J-3\tau/2$ (see Eqs. (11) and (12) in which one should set $P_{dc}=0$).

The second case is represented by the two pairs of orbital singlets having $S=0$, namely by the $(1,1)0$ and $(0,0)0$ – pairs whose adiabatic potentials are given by Eqs. (13) and (14), respectively, upon substituting $P_{dc}=0$ into these expressions. An important difference from the above discussed situation is that now the electronic levels in each pair are separated by a gap which is $2\Delta_1=4\tau$ for the $(1,1)0$ pair and $2\Delta_2=6\tau$ for the $(0,0)0$ pair. The two states within each pair are mixed by the vibronic coupling giving rise to a typical picture of the pseudo - JT effect. Depending on the relationship between the off-diagonal (resonant) contribution of the DE defining the gap 2Δ ($\Delta=\Delta_1$ or Δ_2 depending on which pair is considered) and the strength of the vibronic interaction, the lower sheet of the adiabatic potential has either two equivalent minima (case of relatively strong vibronic coupling when $v^2/\hbar\omega>\Delta$) at the points

$$q_{1,2}=\pm\sqrt{\frac{v^2}{\hbar^2\omega^2}-\frac{\Delta^2}{v^2}} \qquad (17)$$

in which the delocalization of the excess electrons is largely suppressed by the vibronic interaction (strong pseudo - JT effect), or a single minimum ($v^2/\hbar\omega<\Delta$) in which electronic pair is fully delocalized over two diagonal positions (weak pseudo - JT effect). Note that the case of pseudo - JT effect in a square-planar MV tetramer has direct analogy with the conventional semiclassical picture of the electron transfer in a dimeric MV systems considered in the framework of PKS model (see also the above discussion of the analogy between the B_{1g} - vibration in a square planar MV tetramer and the odd out-of-phase mode in a MV dimer). The overall semiclassical energy pattern of the $d^2-d^2-d^1-d^1$-type cell represents a composition of the adiabatic potentials arising from both static JT effect and pseudo - JT effect.

The vibronic coupling results in stabilization of all spin-vibronic states (energies of the minima of the adiabatic potentials) as compared with pure electronic states (energies at *q*=0), with this stabilization being maximal for the states exhibiting JT effect and less pronounced for those related to the pseudo - JT effect. Moreover, different spin-states exhibiting pseudo-JT effect can possess different vibronic stabilization energies, because the latter are dependent on the strength of pseudo-JT effect. The above arguments create a strong conviction that the vibronic coupling, if it is strong enough, should be able to change the order of the energy levels

as compared with that found in the case of zero or weak vibronic coupling (or found in the framework of pure electronic approach) and particularly to have the ability of changing the ground state of the free cell.

To justify the validity of the above statement we plot in Fig. 6 some selected examples of the adiabatic potentials of the free $d^2-d^2-d^1-d^1$-type cell evaluated at different relative values of the electronic parameters (parameters of DE and HDVV exchange) and different values of the vibronic coupling parameter. The values of parameters in these examples are chosen in such a way that the variation of the strength of the vibronic coupling would be able to cause a crossover of different low-lying spin-vibronic levels, the role of which

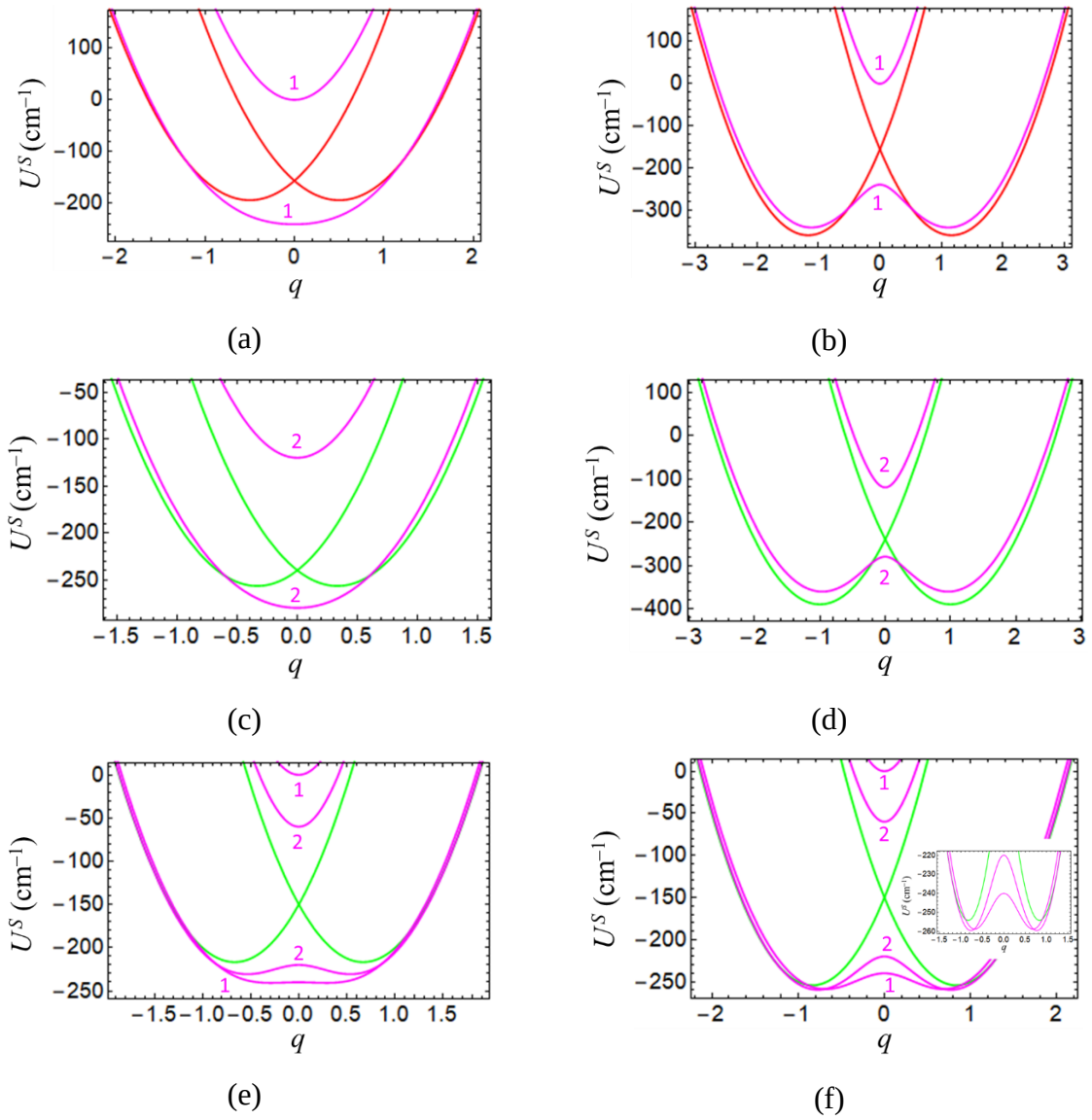

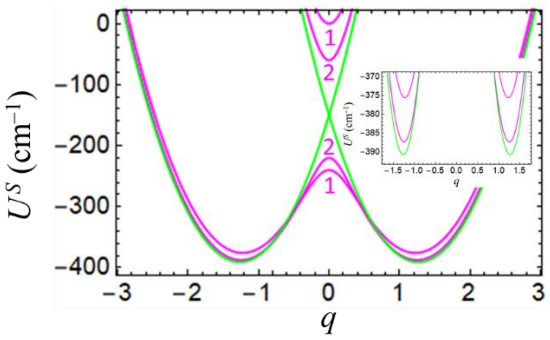

(g)

Figure 6. Schemes of the adiabatic potentials of the free square-planar cell of $d^2 - d^2 - d^1 - d^1$-type evaluated with $\hbar\omega = 300$ cm^{-1}, $\tau = 40$ cm^{-1} and the following sets of J and υ values: J = –1 cm^{-1}, υ = 150 cm^{-1} (a); J = –1 cm^{-1}, υ = 350 cm^{-1} (b); J = –30 cm^{-1}, υ = 100 cm^{-1} (c); J = –30 cm^{-1}, υ = 300 cm^{-1} (d); J = –15 cm^{-1}, υ = 200 cm^{-1} (e); J = –15 cm^{-1}, υ = 250 cm^{-1} (f); J = –15 cm^{-1}, υ = 380 cm^{-1} (g). Only selected adiabatic potentials which can give rise to the ground states (associated with the minima) at different parametric regimes are shown. Coloring and labelling of the states are the same as in the electronic correlation diagram (Fig. 3).

are played by the minima of the lower adiabatic potential curves in the framework of semiclassical approximation. Note that the value $\tau = 40$ cm^{-1} used in the plots in Fig. 6 falls within its range determined by using the t values found for some recently reported weakly coupled MV clusters [52, 53]. Thus for $[Fe_2]^V$ complex the DE parameter has been found to be $B = t/(2S_0 + 1) \approx 69$ cm^{-1} [53] and hence $t \approx 416$ cm^{-1} for $S_0 = 5/2$. For square tetramer with the shortest intermetallic distance of ≈ 8 Å (the same as the intermetallic distance in the $[Fe_2]^V$ dimer) the estimated intracell Coulomb energy U proves to be ≈ 4235 cm^{-1} and so the inequality $t << U$ is fulfilled, with the corresponding second-order DE parameter being equal to $\tau \approx 40.86$ cm^{-1} that is close to the value 40 cm^{-1} we use in our calculations. Depending on the intermetallic distances and the bridging angles in the weakly coupled transition metal clusters the values of HDVV exchange parameter typically vary from several wavenumbers [52, 53] to several tens wavenumbers [54] and so the values of J used here fall within the reasonable range of values. Finally, the vibronic stabilization energies evaluated with the used values of υ and $\hbar\omega$ prove to be much smaller than the Coulomb gap U and so the second inequality $\upsilon^2/(2\hbar\omega) \ll U$ defining the applicability of the present vibronic approach is also rather well satisfied.

Figures 6a and 6b show selected adiabatic potential curves evaluated at relatively strong DE when $|J|/\tau = 1/40$, namely the curves arising from the orbital doublet with *S*=3 (state exhibiting static JT effect) and those arising from a pair of orbital and spin singlets of $((0,0)0)$-type showing pseudo-JT effect. For relatively weak vibronic coupling (case shown in Fig. 6a) the ground adiabatic state is that having *S*=0 (state 1) exactly as in the case of zero vibronic coupling (see left part of electronic correlation diagram in Fig. 3). This ground state can be thought as that in the minimum of the single-well adiabatic potential curve typical for weak pseudo-JT effect that occurs at $\upsilon^2/\hbar\omega < \Delta$. It is seen from Fig. 6a that at weak vibronic coupling the *S*=3 - state represented by the two intersecting parabolas is excited. For stronger vibronic coupling with $\upsilon = 350\ \mathrm{cm}^{-1}$ we are dealing with the case of strong pseud-JT effect for the spin-singlet state for which the lower branch of the adiabatic potential has double well shape shown in Fig. 6b. One can see that although the increase of the vibronic coupling results in the stabilization of minima of the adiabatic potentials with both *S*=0 and *S*=3, stabilization energy for the *S*=3 - state is stronger than that for the *S*=0 – state. This is evidently due to the aforenamed physical difference between the JT-effect promoting full localization in the minima and the pseudo-JT effect, in which case the effective DE hinders vibronic localization of the excess electrons. As a result, instead of the ground spin-singlet occurring in systems with relatively strong DE and weak vibronic coupling, in systems exhibiting the same relative strength of the DE and HDVV exchange but much stronger vibronic coupling the ground state proves to be that with *S*=3 (Fig. 6b). This example shows that vibronic coupling can play a pivotal role, particularly it can stabilize the state with *S* = 3, which by no means can be predicted to be a ground state provided that the tetramer is treated within the pure electronic approach.

Similar effect of the vibronic coupling on the ground spin-state occurs at $|J|/\tau = 3/4$, (see Figs. 6c, 6d) which is the case of relatively weak double exchange when the ground state of the free cell at weak vibronic coupling (Fig. 6c) is the lower of two orbital $((1,1)0)$)-singlets (spin singlet 2) showing pseudo-JT mixing by the B_{1g} -mode, while the first excited state is the orbital doublet with *S*=1 giving rise to the JT effect. Since the JT stabilization dominates over the pseudo-JT the ground state with *S*=0 that occurs in cells with weak vibronic coupling (Fig. 6c) changes to that with *S*=1 for cells in which vibronic coupling is enough enhanced (Fig. 6d). In this example the effect of the increase of the vibronic coupling is somewhat similar to the effect of the increase of $|J|/\tau$ (i. e. to decreasing of the relative strength of the DE) in the electronic correlation diagram, Fig. 3.

Figures 6d-6f show the case of $|J|/\tau = 3/8$ (moderate DE) when at weak vibronic coupling the ground state is the spin-singlet $((0,0)0)$ (spin-singlet 1), the first excited state is another spin-singlet $((1,1)0)$) (spin-singlet 2), and the second excited state is the spin-triplet as shown in Fig. 6d. The two pairs of spin-singlets each demonstrates the pseudo-JT effect, with such an effect being stronger for the $((1,1)0)$) - pair than for the $((0,0)0)$ - one because of smaller electronic gap Δ for the $((1,1)0)$)-pair (4τ against 6τ). Upon increasing of υ the ground state first changes from the spin-singlet 1 to the spin-singlet 2 because of more pronounced pseudo-JT stabilization of the state 2 (Fig. 6e), while the further increase of the vibronic coupling gives rise to the ground spin-triplet state as a result of its dominating JT stabilization (Fig. 6f).

By comparing the above discussed effects of the vibronic coupling (Fig. 6) with those produced by the electrostatic field of polarized driver-cell on the working cell in which the vibronic coupling is zero (see the discussion at the end of Section 2) one can conclude that the vibronic coupling and the electrostatic field can produce the same kinds of switching between different spin-states. Such similarity of the two kinds of effects and its role in the functional properties of the cells will be discussed in the next Section in more details in the framework of more exact quantum-mechanical vibronic approach.

When the field of the driver is switched on ($P_2 \neq 0$) the JT problem for the *S*=3 pair remains static which means that the adiabatic potentials are still represented by the two intersecting parabolic curves

$$U_{D_1}((2,1)3, P_2|q) = -4J - 4\tau + \frac{\hbar\omega}{2}(q - q_0)^2 - \Delta E - uP_2, \quad (18)$$

$$U_{D_2}((1,2)3, P_2|q) = -4J - 4\tau + \frac{\hbar\omega}{2}(q + q_0)^2 - \Delta E + uP_2. \quad (19)$$

which are shifted up and down by the value uP_2 due to the interaction of the working cell with the polarized driver-cell. This means that the action of the field does not violate the static nature of the JT effect, but only makes the two minima energetically inequivalent, retaining unchanged their positions given by Eq. (17) and also electronic distribution in each minimum. This means that the effect of the field on the *S*=3 - state consists in stabilization of one antipodal position accompanied by destabilization of another one and the same is true for the JT-type spin-triplet state. In contrast, the field of the driver-cell essentially affects both positions and the depths of the minima of the pseudo-JT-type lower adiabatic curves with $S = 0$, as well as the electronic densities in these minima.

The evaluation of the field dependences of the adiabatic potentials and the adiabatic wave-functions in the minima at different sets of τ, J and υ - values allows us, in principle, to perform numerical analysis of the effect of the vibronic coupling on the field-induced spin-switching and also on the shape of semiclassical cell-cell response function. However, due to the approximate character of semiclassical approach which fails to catch such important quantum phenomena as tunneling of the electrons, it seems to be preferable to perform the quantitative study of the properties of the cell in the framework of more precise quantum-mechanical vibronic approach. This will be done in the next Section.

5. Properties of cells in the framework of quantum-mechanical vibronic approach

Although the adiabatic approach provides a qualitatively correct picture illustrating the main features of the systems under consideration it has restricted applicability for quantitative description of the spin-switching phenomena and cell-cell response, especially in the case of moderate vibronic coupling when the quantum tunneling of the electrons cannot be neglected [48]. This mainly refers to the situations in which the physical processes of interest occurs at the atomic configurations corresponding to the vicinity of avoided crossing (or avoided crossing) regions because just in such regions the quantum tunneling processes strongly influence the reorientation of the antipodal charge configurations and consequently affects the cell-cell response function in the most important area of its nonlinearity. To overcome such limitations of semiclassical approximation in this Section we apply the quantum-mechanical approach to the vibronic problem. This means that we have to solve the eigen-problem of the full Hamiltonian taking into account the kinetic energy of the vibrations (that is why it is appropriate to call this approach dynamic). Evaluation of the eigen-system is performed through the diagonalization of the full Hamiltonian of the tetrameric cell whose matrix form is defined in the basis

$$\langle D_1\,(S_{13})(S_{24})\;S\;M|\,\langle n|\;,\;\langle D_2\,(S_{13})(S_{24})\;S\;M|\langle n| \qquad (20)$$

composed of the products of the electronic wave-functions with definite spin quantum numbers belonging to the two diagonal configurations D_1 and D_2 and the wave-functions of the free harmonic oscillator (n = 0, 1, ...) which are the eigen-functions of the Hamiltonian $\widehat{H}_0$ in Eq. (8). Then we perform truncation of the vibrational basis in order to avoid the necessity to diagonalize the infinite size matrix. The dimension of the vibrational basis (maximal number $n = n_{max}$) is chosen to ensure a good enough convergence of the results that means that the further increase of the space produces negligible affects the energies of the low-lying vibronic

levels. The required number n_{max} increases with the increase of the vibronic coupling parameter and also depends on the strength of the quadrupole field when the interaction of the working cell with the driver-cell is included in the consideration. This especially refers to the energy region near the avoided crossing of the adiabatic potentials interrelated with the fast switching between the two antipodal charge configurations of the working cell under the action of the driver-cell. While performing the calculation of the spin-vibronic levels we fix the maximal quantum number of the harmonic oscillator at n_{max} = 100, which proves to be large enough vibrational space to ensure good convergence of the numerical solution of the dynamic vibronic problem (at least it is enough to evaluate the low-lying vibronic states which are important for the analysis of the low-temperature properties of the cell) in the full ranges of the used values of the vibronic coupling parameter and the driver-cell polarization.

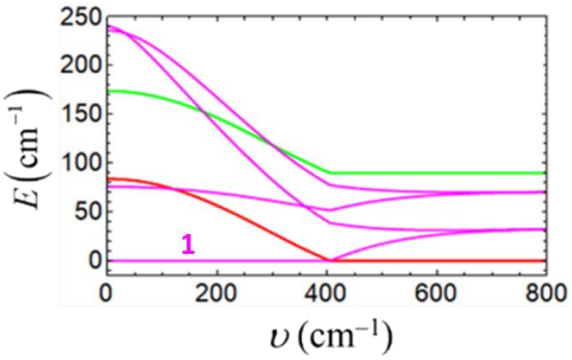

(a)

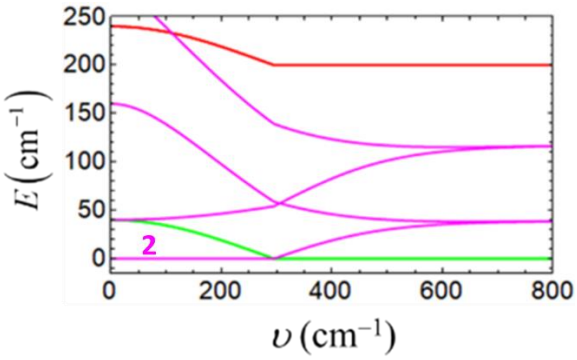

(b)

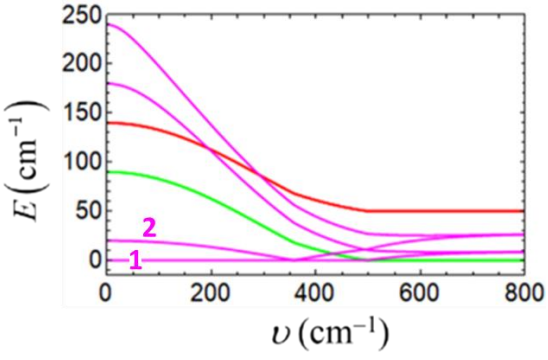

(c)

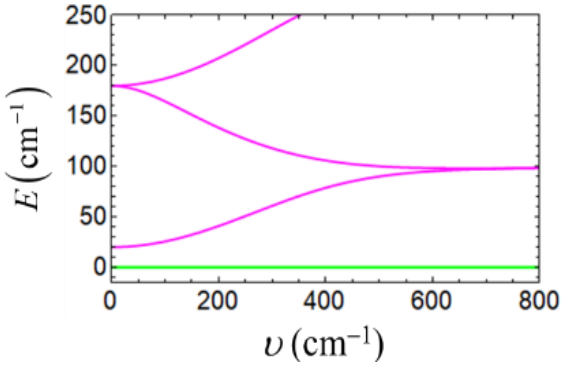

(d)

Figure 7. Dependences of the energies of low-lying spin-vibronic levels of an isolated square-planar of the $d^2-d^2-d^1-d^1$-type cell on the vibronic parameter υ calculated with $\hbar\omega = 300\ \mathrm{cm}^{-1}$, $\tau = 40\ \mathrm{cm}^{-1}$ and $J = -1\ \mathrm{cm}^{-1}$(a), $J = -30\ \mathrm{cm}^{-1}$ (b), $J = -15\ \mathrm{cm}^{-1}$ (c), and $J = -60\ \mathrm{cm}^{-1}$ (d). The ground vibronic level is chosen as a reference point for the energy. Only the energies of those states are shown which are the ground ones in an isolated or fully polarized cell. Coloring and labelling of the spin-states are the same as in Fig. 3.

Figure 7 shows the energies of the low-lying spin-vibronic states of the free cell evaluated as functions of the vibronic coupling parameter υ at fixed sample parameters $\hbar\omega = 300\ \mathrm{cm}^{-1}$, $\tau = 40\ \mathrm{cm}^{-1}$ and four different values of *J*. When the DE significantly exceeds the HDVV exchange (case shown in Fig. 7a) the ground state of the cell is a spin singlet 1 for weak vibronic coupling. It is seen that the increase of υ leads to the decrease of the gap between the states with *S* = 0 to *S* = 3 and at a certain critical value $\upsilon \approx 400\ \mathrm{cm}^{-1}$ the ground state changes to that with *S* = 3. Note that although this effect of the vibronic coupling is qualitatively the same as that predicted in the framework of the adiabatic approach (see the upper plots in Fig. 6) the change of the ground state occurs at higher critical value of υ as compared with that predicted by semiclassical approach. Indeed, it is seen from Fig. 6 that at $\upsilon \approx 350\ \mathrm{cm}^{-1}$ the ground adiabatic state is already that having *S* = 3 for the same values of the electronic parameters. This quantitative deviation between quantum-mechanical and semiclassical treatments can be explained by the essentially quantum phenomenon of tunneling between the minima, which by no means can be taken into account within the semiclassical approximation. Such tunneling has destructive influence on the vibronic self-trapping effect and, therefore, to reach the point of changing of the ground spin-state a larger value of the vibronic coupling is required.

For $J = -30\ \mathrm{cm}^{-1}$ vibronic coupling upon increasing tends to change the ground spin-singlet 2 to the spin-triplet as can be seen from Fig. 7b, and at $J = -15\ \mathrm{cm}^{-1}$ the increase of the vibronic coupling first (at $\upsilon \approx 360\ \mathrm{cm}^{-1}$) changes the ground spin-singlet 1 to the spin-singlet 2 and then (at $\upsilon \approx 500\ \mathrm{cm}^{-1}$) the ground spin-singlet 2 is changed to the ground spin-triplet (Fig. 7c). These kinds of behavior are also qualitatively similar to those found within the adiabatic approach as can be seen from comparison of Figs. 7b and 7c with the adiabatic potentials in Fig. 6 calculated with the same sets of τ and *J* values. These examples also demonstrate that the quantum-mechanical approach leads to the conclusion about stronger

vibronic coupling required for producing switching between different spin-states than that predicted by the semiclassical approach.

Finally, in the case of relatively weak DE shown in Fig. 7d the ground spin-vibronic state is a JT-type S=1 – state. The increase of the vibronic coupling cannot change this ground state but only leads to its additional stabilization with respect to the first excited pseudo-JT-type state with S = 0.

Calculated dependences of the spin-vibronic energy levels on υ presented in Fig. 7 fully confirm the conclusion above drown on the basis of the adiabatic approximation about physical similarities between the effects of the electrostatic quadrupole field and the vibronic coupling on the ground spin-state of the cell. This similarity is closely related to the physical nature of these two interactions, which both promote localization of the electronic pair along one of the diagonals of the square. Indeed, both these interactions suppress the resonant (off-diagonal) second-order DE contributions producing mixing of the orbital singlets with opposite parities, and also split the orbital doublets. At the same time the important difference between the effects of the quadrupole field and the vibronic coupling on the polarization of the cell should be pointed out, namely, strictly speaking only the former interaction can produce genuine polarization of the cell by creating predominant localization along one of the diagonals, while the vibronic interaction polarizes the cell only in the sense of broken symmetry, i. e. when one of the two equivalent minima of the adiabatic potentials is selected. Still, vibronic coupling produces part of the work on the cell polarization by forming the predominant localization in the minima. If such minima are deep enough and so the tunneling splitting of the low-lying vibronic levels are not so large the remaining work the field has to perform is getting strongly facilitated because the field in this case only needs to induce asymmetry (inequivalence) of the minima and to suppress residual tunneling. In other words, the vibronic interaction effectively amplifies the polarizability of the cell. Such vibronic amplification can be termed “the effect of the vibronic enhancement of the cell-cell interaction”.

It is reasonable to expect that the vibronic amplification effect can produce significant impact both on the conditions for field-induced switching between different spin-states and on the character of the cell-cell response function. To clarify this point we have plotted in Fig. 8 the dependences of the low-lying spin-vibronic energy levels on the driver-cell polarization P_{dc} calculated for fixed $\hbar\omega$, τ and u values and different sets of J and υ values. The used value u = 250 cm^{-1} can be regarded as reasonable estimation of the intercell Coulomb energy for typical intra- and intercell distances as discussed in ref. [33]. Figures 8a and 8b describe the case of

relatively strong DE, when this interaction significantly exceeds the HDVV exchange. One can see that in the case of a weak vibronic coupling, the Coulomb field induces spin switching S = 0→ S = 3 (Fig. 8a), while in the case of a strong coupling, the state with S = 3 proves to be the ground state already at P_{dc} = 0 and it remains the ground one at all P_{dc} values (Fig.8b). Figures 7c-f show the dependences of the energy spectra vs polarization P_{dc} calculated at $J = -15$ cm^{-1} and four increasing values of the parameter υ. It is seen that the enhancement of the vibronic coupling leads to the decrease of the critical values of P_{dc} required to switch the spin-singlet 1 to the spin-singlet 2 and then to induce the spin-switching from the spin-singlet 2 to the spin-triplet. Finally, at strong enough vibronic coupling,

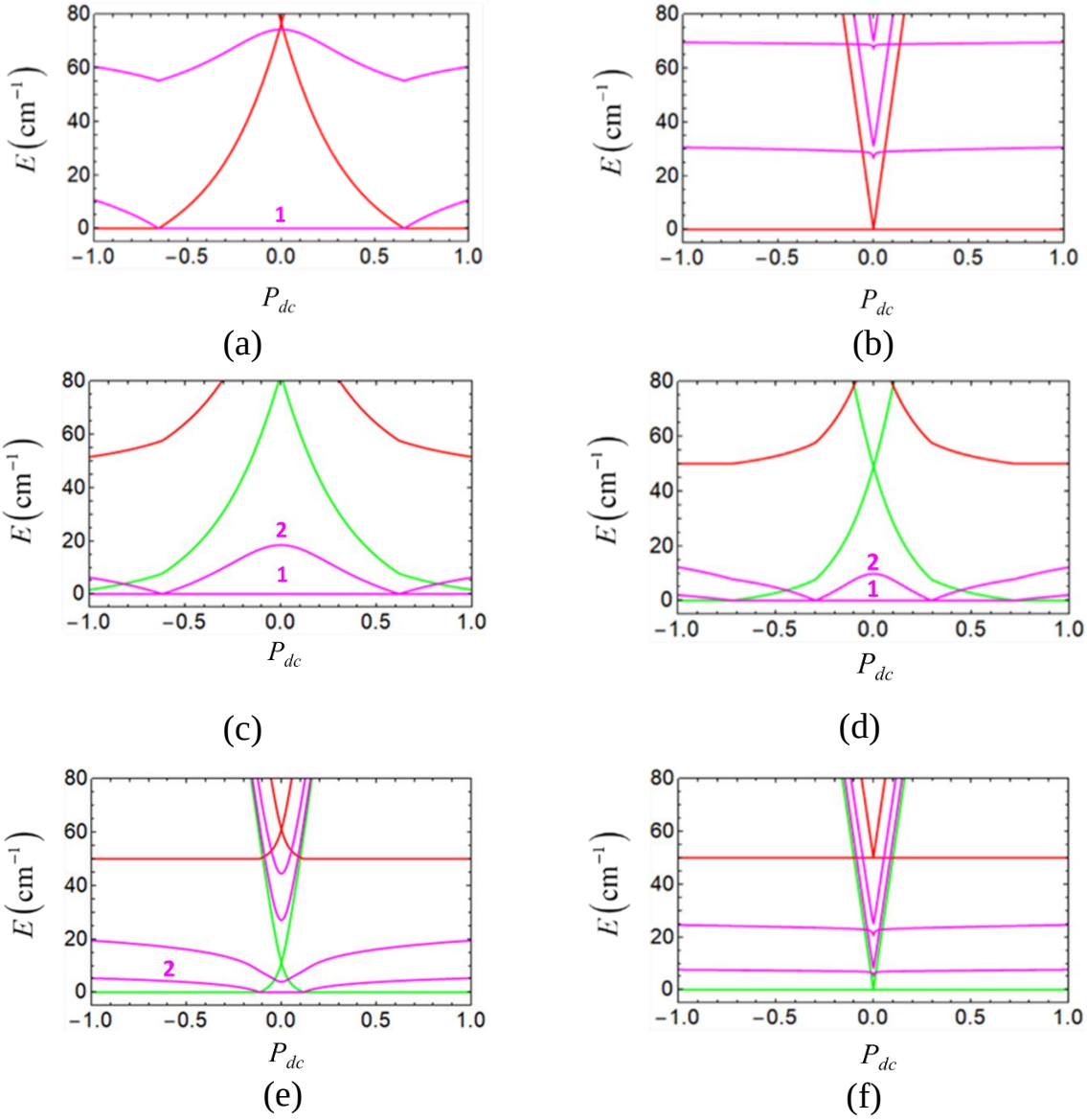

Figure 8. Dependences of the energies of low-lying spin-vibronic levels of square-planar cell of $d^2 - d^2 - d^1 - d^1$ -type on the polarization P_2 of the driver-cell calculated for $\hbar\omega = 300\ \mathrm{cm}^{-1}, \tau = 40\ \mathrm{cm}^{-1}, u = 250\ \mathrm{cm}^{-1}$and the following sets of parameters J and υ: $J = -1\ \mathrm{cm}^{-1}, \upsilon = 100\ \mathrm{cm}^{-1}$ (a) , $J = -1\ \mathrm{cm}^{-1}, \upsilon = 600\ \mathrm{cm}^{-1}$ (b), $J = -15\ \mathrm{cm}^{-1}$, $\upsilon = 100\ \mathrm{cm}^{-1}$ (c), $J = -15\ \mathrm{cm}^{-1}, \upsilon = 250\ \mathrm{cm}^{-1}$ (d), $J = -15\ \mathrm{cm}^{-1}, \upsilon = 400\ \mathrm{cm}^{-1}$ (e), $J = -15\ \mathrm{cm}^{-1}$, $\upsilon = 600\ \mathrm{cm}^{-1}$ (f). The ground spin-vibronic level is chosen as a reference point for the energy. Only the energies of those states are shown, which can be the ground states in the isolated or fully polarized cell.

the vibronic interaction itself (that is, without support of the quadrupole field) is able to stabilize the spin-triplet, which then remains the ground state at any P_{dc} values (Fig. 8f).

Analysis of the calculated shapes of the "vibronic" cell-cell response functions shown in Fig. 9 allows to reveal an additional feature of spin-switching interrelated with the vibronic

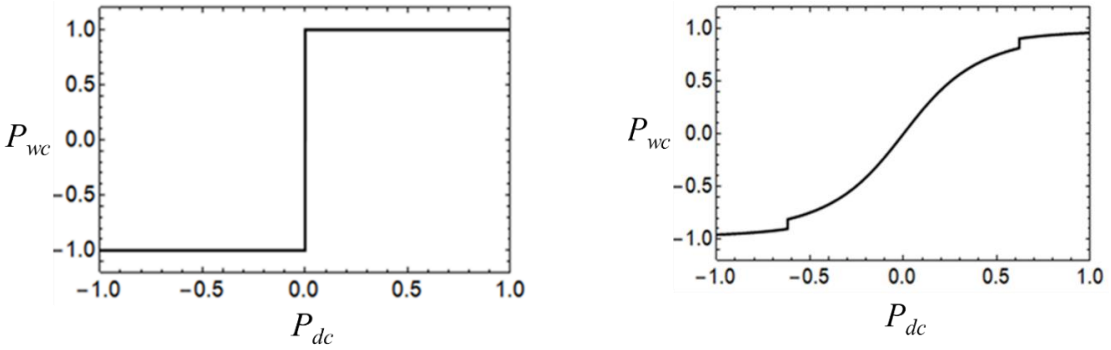

(a) (b)

Figure 9. Cell-cell response functions calculated in the low-temperature limit for $\hbar\omega =$ cm^{-1}, $\tau = 40\ \mathrm{cm}^{-1}$, $J = -15\ \mathrm{cm}^{-1}$, $u = 250\ \mathrm{cm}^{-1}$ and $\upsilon = 400\ \mathrm{cm}^{-1}$ (a) and $\upsilon = 100\ \mathrm{cm}^{-1}$ (b).

interaction. These cell-cell response functions are calculated in the low-temperature limit when only the ground spin-vibronic level is thermally populated. The spin-singlets and spin-triplet possess different polarizabilities due to the fact that spin-singlets are the states exhibiting pseudo-JT effect while the spin-triplet is a JT-state. For this reason, the spin-switching from the state with $S = 0$ to that with $S = 1$ is expected to lead to the abrupt change of P_{wc} and the same kind of behavior can be expected due to the spin-switching $S = 0 \rightarrow S = 1$. Moreover, the spin-singlets 1 and 2 are also characterized by different polarizabilities and hence the switching between two spin-singlets should also be accompanied by the abrupt change of P_{wc} in spite of

the fact that in this case the total spin of the cell does not change. Just these kinds of stepwise behavior of cell-cell response function have been predicted while considering the cell in the framework of pure electronic model [34]. Based on these previous results one would expect, that, for example, in the case of spin switching depicted in Fig.8e an abrupt change in P_{wc} should occur at that value of $|P_{dc}|$ at which the cell undergoes switching from the spin-singlet state demonstrating the quadratic Stark effect to the spin-triplet state for which the Stark effect is linear. Unlike such expectation, P_{wc} saturates at $|P_2|$ which is much less than the value at which spin switching occurs (Fig. 9a). This discrepancy between the electronic and vibronic cell-cell response functions is explained by the fact that providing such strong vibronic interaction, the difference between the effect and pseudo-JT effect can be neglected and so the Stark effect for the spin-singlet becomes linear and so the differences in polarizabilities of spin-singlet and spin-triplet disappears. Alternatively, one can say that in this case the resonant splitting of the orbital doublet with $S = 0$ caused by the second-order DE is completely suppressed by the vibronic coupling. In contrast, in the case of a relatively weak vibronic interaction, the Stark effect differs significantly for different spin states, which leads to a stepwise change of P_1 when the ground state of the cell is changed (see Figs. 9b and 8c).

Conclusions

In summary, several results of the present vibronic theory of the square-planar cells containing four spin cores interacting with a pair of excess electrons should be noted. It has been shown that in the important limiting case when the hierarchy of the key intracell interactions is described by the inequalities $\upsilon^2/(2\hbar\omega),\ |t| \ll U$ the complex multimode vibronic problem including interaction of the excess electrons with four local breathing modes is reduced to a single-mode vibronic problem in which the active mode is the molecular PKS-type B_{1g} -vibration. The detailed analysis of the vibronic effects has been performed for the isolated and interacting square planar-cells based on MV transition metal tetramer of the $d^2 - d^2 - d^1 - d^1$ type although the conceptual conclusions made in course of this study can be also applied to more complex multielectron cells. The interaction of the excess electrons with B_{1g} - mode has been shown to lead to the JT problem for the spin-states which are the localized orbital doublets (like considered states with S=1 and S=3) and to the pseudo-JT problem for the pairs of orbital singlets having opposite parities and the same sets of spin quantum numbers (these are the states with S=0 arising from different sets of intermediate spins).

An analysis of the found energies of the adiabatic potentials' minima, as well as of the dependences of the spin-vibronic energy levels of a free cell on the vibronic coupling parameter

obtained by solving numerically the dynamic vibronic problem, has allowed us to conclude that the vibronic coupling in a free cell produces an effect, which is quite similar to the effect produced by the driver-cell when it acts on the working cell. A consequence of this is that in the case of strong vibronic coupling one should significantly modify the conclusions earlier drawn on the basis of a purely electronic model and related to the possible types of the ground spin states in a free cell and the conditions for their stabilization under the action of the electrostatic field created by the driver-cell. In particular, we have shown that in the case when both vibronic coupling and the second order DE act as relatively strong interactions the ground state of a free cell is a state with spin $S = 3$, which by no means can appear as a ground state provided that the vibronic interaction is weak.

For interacting cells, the vibronic coupling significantly amplifies the ability of the electrostatic field of the driver-cell to polarize the working cell. This effect, which we termed "the vibronic enhancement of the cell-cell interaction", leads to a redetermination of the conditions for switching between different spin-states, as well as to a significant change in the shapes of the cell-cell response functions, which should be taken into account in the problem of rational design of multielectron cells suitable for creating QCA devices and spin switches. These results underline the importance of the vibronic coupling in all aspects (such as description of an isolated cell and cell-cell response) of the theory of molecular QCA based on MV clusters. Finally, it is worthwhile to note that the systems considered in this article are expected to exhibit magnetoelectric coupling and therefore can be referred to as belonging to the special class of single-molecule magnetoelectrics discussed in detail in Ref. [55].

Acknowledgements

The work was performed with financial support from Russian Science Foundation (project No. 20-13-00374) in the Laboratory of Molecular Magnetic Nanomaterials established within the agreement between the Ministry of Science and Higher Education of the Russian Federation and the Institute of Problems of Chemical Physics, Chernogolovka (Agreement No. 14.W03.31.0001).

References

[1] C. S. Lent, P. D. Tougaw, W. Porod, G. H. Bernstein, Quantum cellular automata, *Nanotechnology* **1993**, *4*, 49 −57.

[2] C. S. Lent, P. D. Tougaw, W. Porod, Bistable saturation in coupled quantum dots for quantum cellular automata, *Appl. Phys. Lett*. **1993**, *62*, 714-716.

[3] C. S. Lent, P. D. Tougaw, Lines of interacting quantum-dot cells: A binary wire, *J. Appl. Phys*. **1993**, *74*, 6227-6233.

[4] C. S. Lent, B. Isaksen, M. Lieberman, Molecular quantum-dot cellular automata, *J. Am. Chem. Soc*. **2003**, *125*, 1056−1063.

[5] B. Tsukerblat, A. Palii, S. Aldoshin, molecule based materials for quantum cellular automata: A short overview and challenging problems, *Israel J. Chem*., **2020,** *60*, 1- 18.

[6] B. Tsukerblat, A. Palii, J.M. Clemente-Juan, N. Suaud, E. Coronado, Quantum cellular automata: a short overview of molecular problem, *Acta Physica Plolonica* A, **2018,** *133*, 329-335.

[7] P. D. Tougaw, C. S. Lent, Logical devices implemented using quantum cellular automata, *J. Appl. Phys*. **1994**, *75***,** 1818-1825.

[8] C. S. Lent, P. D. Tougaw, A device architecture for computing with quantum dots. *Proc. IEEE*, **1997**, *85*, 541 - 557.

[9] W. Porod, C. S. Lent, G. H. Bernstein, A. O. Orlov, I. Amlani, G. L. Snider, J. L. Merz, Quantum-dot cellular automata: computing with coupled quantum dots, *Int. J. Electronics*, **1999**, *86*, 549 - 590.

[10] G. Tóth, C. S. Lent, Quasiadiabatic switching for metal-island quantum-dot cellular automata, *J. Appl. Phys*., **1999**, *85*, 2977-2984.

[11] G. Tóth, C. S. Lent, Quantum computing with quantum-dot cellular automata, *Phys. Rev. A*. **2001**, *63*, 052315 (1-8).

[12] C. S. Lent, Bypassing the transistor paradigm, *Science*, **2000**, *288*, 1597−1599.

[13] K. Hennessy, C. S. Lent, Clocking of molecular quantum-dot cellular automata, *J. Vac. Sci. Technol., B: Microelectron. Process. Phenom*., **2001**, *19*, 1752−1755.

[14] J. Jiao, G. J. Long, F. Grandjean, A. M. Beatty T. P. Fehlner, Building blocks for the molecular expression of quantum cellular automata. isolation and characterization of a covalently bonded square array of two ferrocenium and two ferrocene complexes. *J. Am. Chem. Soc.*, **2003**, *125*, 7522−7523.

[15] Z. Li, A. M. Beatty, T. P. Fehlner, Molecular QCA cells. 1. Structure and functionalization of an unsymmetrical dinuclear mixed-valence complex for surface binding. *Inorg. Chem*., **2003**, *42*, 5707−5714.

[16] Z. Li,. T. P. Fehlner, Molecular QCA cells. 2. Characterization of an unsymmetrical dinuclear mixed-valence complex bound to a Au surface by an organic linker, *Inorg. Chem*., **2003**, *42*, 5715−5721.

[17] H. Qi, S. Sharma, Z. Li, G. L. Snider, A. O. Orlov, C. S. Lent, T. P. Fehlner, Molecular quantum cellular automata cells. Electric field driven switching of a silicon surface bound array of vertically oriented two-dot molecular quantum cellular automata, *J. Am. Chem. Soc*., **2003**, *125*, 15250−15259.

[18] S. B. Braun-Sand, O. Wiest, Theoretical studies of mixed valence transition metal complexes for molecular computing, *J. Phys. Chem. A* **2003**, *107*, 285−291.

[19] S. B. Braun-Sand, O. Wiest, Biasing mixed-valence transition metal complexes in search of bistable complexes for molecular computing, *J. Phys. Chem. B* **2003**, *107*, 9624−9628.

[20] H. Qi, A. Gupta, B. C. Noll, G. L. Snider, Y. Lu, Lent, C.; T. P. Fehlner, Dependence of field switched ordered arrays of dinuclear mixed-valence complexes on the distance between the redox centers and the size of the counterions, *J. Am. Chem. Soc*. **2005**, *127*, 15218−15227.

[21] J. Jiao, G. J. Long, L. Rebbouh, F. Grandjean,; A. M. Beatty, T. P. Fehlner, Properties of a mixed-valence $(Fe^{II})_2(Fe^{III})_2$ square cell for utilization in the quantum cellular automata paradigm for molecular electronics, *J. Am. Chem. Soc*. **2005**, *127*, 17819−17831.

[22] Y. Lu, C. S. Lent, Theoretical study of molecular quantum dot cellular automata. *J. Comput. Electron*. **2005**, *4*, 115−118.

[23] Y. Zhao, D. Guo, Y. Liu, C. He, C. Duan, A mixed-valence $(Fe^{II})_2(Fe^{III})_2$ square for molecular expression of quantum cellular automata, *Chem. Commun*. **2008**, 5725−5727.

[24] V. N. Nemykin, G. T. Rohde, C. D. Barrett, R. G. Hadt, C. Bizzarri, P. Galloni, B. Floris, I. Nowik, R. H. Herber, A. G. Marrani,. et al. Electron-transfer processes in metal-free tetraferrocenylporphyrin. understanding internal interactions to access mixed valence states potentially useful for quantum cellular automata, *J. Am. Chem. Soc*. **2009**, *131*, 14969−14978.

[25] X. Wang, L. Yu, V. S. S. Inakollu, X. Pan, J. Ma, H. Yu, Molecular quantum-dot cellular automata based on diboryl radical anions, *J. Phys. Chem. C* **2018**, *122*, 2454–2460.

[26] A. Burgun, F. Gendron, P. A. Schauer, B. W. Skelton, P. J. Low, K. Costuas, J.-F. Halet, M. I. Bruce, C. Lapinte, Straightforward access to tetrametallic complexes with a square array by oxidative dimerization of organometallic wires, *Organometallics* **2013**, *32*, 5015−5025.

[27] B. Schneider, S. Demeshko, S. Neudeck, S. Dechert, F. Meyer, Mixed-spin [2 × 2] Fe_4 grid complex optimized for quantum cellular automata, *Inorg. Chem*., **2013**, *52*, 13230−13237.

[28] J. A. Christie, R. P. Forrest, S. A. Corcelli, N. A. Wasio, R. C. Quardokus, R. Brown, S. A. Kandel, Y. Lu, C. S. Lent, K. W. Henderson, Synthesis of a neutral mixed-valence diferrocenyl carborane for molecular quantum-dot cellular automata applications, *Angew. Chem., Int. Ed*., **2015**, *54*, 15448−15671.

[29] R. Makhoul, P. Hamon, T. Roisnel, J.-R. Hamon, C. Lapinte, A tetrairon dication featuring tetraethynylbenzene bridging ligand: a molecular prototype of quantum dot cellular automata, *Chem. Eur. J.*, **2020**, *26*, 8368 – 8371.

[30] A. Palii, S. Aldoshin, S. Zilberg, B. Tsukerblat, Parametric two-mode vibronic model of a dimeric mixed valence cell for molecular quantum cellular automata and computational ab-initio verification, *Phys.Chem.Chem.Phys*., **2020**, *22*, 25982—25999.

[31] A. Palii, S. Zilberg, A. Rybakov, B. Tsukerblat, Double-dimeric versus tetrameric cells for quantum cellular automata: a semiempirical approach to evaluation of cell−cell responses combined with quantum-chemical modeling of molecular structures, *J. Phys. Chem. C*, **2019**, *123*, 22614−22623.

[32] V. C. Lau, L. A. Berben, J. R. Long, $[(Cyclen)_4Ru_4(pz)_4]^{9+}$: A Creutz-Taube Square, *J. Am. Chem. Soc*. **2002**, *124*, 9042-9043.

[33] A. Palii, J. M. Clemente-Juan, A. Rybakov, S. Aldoshin, B. Tsukerblat, Exploration of the double exchange in quantum cellular automata: proposal for a new class of cells. *Chem. Commun.* **2020**, *56*, 10682-10685.

[34] A. Palii, J. M. Clemente-Juan, S. Aldoshin, D. Korchagin, A. Rybakov, S. Zilberg, B. Tsukerblat, Mixed-valence magnetic molecular cell for quantum cellular automata: prospects of designing multifunctional devices through exploration of double exchange, *J. Phys. Chem. C* **2020**, *124*, 25602–25614.

[35] A. Palii, J. M. Clemente-Juan, S. Aldoshin , D. Korchagin, E. Golosov, S. Zilberg, B. Tsukerblat, Can the double exchange cause antiferromagnetic spin alignment?, *Magnetochemistry* **2020**, *6*, 36-47.

[36] N. S. Hush, Adiabatic theory of outer sphere electron-transfer reactions in solution. Trans. *Faraday Soc.*, **1961**, *57*, 557−580.

[37] N. S. Hush, Distance dependence of electron transfer rates, *Coord. Chem. Rev*. **1985**, *64*, 135−157.

[38] B. S. Brunschwig, N. Sutin, Energy surfaces, reorganization energies and coupling elements in electron transfer, *Coord. Chem. Rev*. **1999**, *187*, 233−254.

[39] K. D. Demadis, Hartshorn, C. M.; Meyer, T. J. The Localized-to-delocalized transition in mixed-valence chemistry, *Chem. Rev*. **2001**, *101*, 2655−2686.

[40] S. B. Piepho, E. R. Krausz, P. N. Schatz, Vibronic coupling for calculation of mixed-valence absorption profiles, *J. Am. Chem. Soc.* **1978**, *100*, 2996−3005.

[41] K. Prassides, P. N. Schatz, Vibronic coupling model for mixed-valence compounds. extension to the multimode case, *J. Phys. Chem*. **1989**, *93*, 83−89.

[42] K. Y. Wong, P. N. Schatz, A dynamic model for mixed-valence compounds, *Prog. Inorg. Chem.*, **1981**, *28*, 369−449.

[43] K. Y. Wong, Charge-transfer-induced IR absorptions in mixed-valence compounds. *Inorg. Chem.*, **1984**, *23*, 1285−1290.

[44] B. Tsukerblat, A. Palii, J.M. Clemente-Juan, Self-trapping of charge polarized states in four-dot molecular quantum cellular automata: bi-electronic tetrameric mixed-valence species, *Pure and Applied Chemistry*, **2015,** *87(3)*, 271–282.

[45] B. Tsukerblat, A. Palii, J.M. Clemente-Juan, E. Coronado, Mixed-valence molecular four-dot unit for quantum cellular automata: vibronic self-trapping and cell-cell response, *J. Chem. Phys.* **2015,** *143*, 134307-15.

[46] A. Palii, B.Tsukerblat, J. M. Clemente-Juan ,E. Coronado, Spin-switching in molecular quantum cellular automata based on mixed-valence tetrameric units, *J. Phys. Chem.* **2016,** *120*, 16994−17005.

[47] J.M. Clemente-Juan, A. Palii, E. Coronado, B. Tsukerblat ,Mixed-Valence Molecular Unit for Quantum Cellular Automata: Beyond the Born-Oppenheimer Paradigm through the Symmetry Assisted Vibronic Approach, *J. Chem. Theory Comp.* **2016,** 12, 3545−3560.

[48] A. Palii, A. Rybakov, S. Aldoshin, B. Tsukerblat, Semiclassical versus quantum-mechanical vibronic approach in the analysis of the functional characteristics of molecular quantum cellular automata, *Phys. Chem. Chem. Phys.* **2019**, *21*, 16751-16761.

[49] C. Zener, Interaction between the d-Shells in the Transition Metals. II. Ferromagnetic compounds of manganese with perovskite structure, *Phys. Rev*. **1951**, *82*, 403−405.

[50] P. W. Anderson, H. Hasegawa, Consideration of double exchange, *Phys. Rev*. **1955**, *100*, 675−681.

[51] P.-G. De Gennes, Effects of double exchange in magnetic crystals, *Phys. Rev.*, **1960**, *118*, 141−154.

[52] B. Bechlars, D. M. D'Alessandro, D. M. Jenkins, A. T. Iavarone, S. D. Glover, C. P. Kubiak, J. R. Long, High-spin ground states via electron delocalization in mixed-valence imidazolate-bridged divanadium complexes. *Nat. Chem*. **2010**, *2*, 362−368.

[53] A. I. Gaudette, I.-R. Jeon, J. S. Anderson, F. Grandjean, G. J. Long, T. D. Harris, Electron Hopping through Double-Exchange Coupling in a Mixed-Valence Diiminobenzoquinone-Bridged Fe_2 Complex, *J. Am. Chem. Soc*. 2015, *137*, 12617–12626.

[54] D. R. Gamelin, E. L. Bominaar, M. L. Kirk, K. Wieghardt, E. I. Solomon, Excited-State Contributions to Ground-State Properties of Mixed-Valence Dimers: Spectral and Electronic-Structural Studies of $[Fe_2(OH)_3(tmtacn)_2]^{2+}$ Related to the $[Fe_2S_2]^{+}$ Active Sites of Plant-Type Ferredoxins, *J. Am. Chem. Soc.* **1996,** *118,* 8085-8097.

[55] A. Palii, S. Aldoshin, B. Tsukerblat, Mixed-valence clusters: Prospects for single-molecule magnetoelectrics, *Coord. Chem. Rev*. **2021,** *426*, 213555 (1-23).